The Astrophysical Journal, 800:122 (14pp), 2015 February 20 doi:10.1088/0004-637X/800/2/122

REVISED MASS-TO-LIGHT RATIOS FOR NEARBY GALAXY GROUPS AND CLUSTERS

Yutong Shan[1,2], Michael McDonald[3,4], and Stéphane Courteau[1]
[1] Department of Physics, Engineering Physics and Astronomy, Queen's University, Kingston, ON, Canada; yshan@cfa.harvard.edu
[2] Now at Harvard-Smithsonian Centre for Astrophysics, 60 Garden Street, Cambridge, MA 02138, USA
[3] Kavli Institute for Astrophysics and Space Research, MIT, Cambridge, MA 02139, USA
Received 2014 March 29; accepted 2014 December 22; published 2015 February 18

ABSTRACT

We present a detailed investigation of the cluster stellar mass-to-light (M^*/L) ratio and cumulative stellar masses, derived on a galaxy-by-galaxy basis, for 12 massive ($M_{500} \sim 10^{14}$–$10^{15}\ M_\odot$), nearby clusters with available optical imaging data from the Sloan Digital Sky Survey Data Release 10 and X-ray data from the *Chandra X-ray Observatory*. Our method involves a statistical cluster membership using both photometric and spectroscopic redshifts when available to maximize completeness while minimizing contamination effects. We show that different methods of estimating the stellar mass-to-light ratio from observed photometry result in systematic discrepancies in the total stellar masses and average mass-to-light ratios of cluster galaxies. Nonetheless, all conversion methodologies point to a lack of correlation between M^*/L_i and total cluster mass, even though low-mass groups contain relatively more blue galaxies. We also find no statistically significant correlation between M^*/L_i and the fraction of blue galaxies ($g-i < 0.85$). For the mass range covered by our sample, the assumption of a Chabrier initial mass function (IMF) yields an integrated $M^*/L_i \simeq 1.7 \pm 0.2\ M_\odot/L_{i,\odot}$, a lower value than used in most similar studies, though consistent with the study of low-mass galaxy groups by Leauthaud et al. A light (diet) Salpeter IMF would imply a ∼60% increase in M^*/L_i.

Key words: galaxies: clusters: general – galaxies: groups: general – galaxies: photometry – galaxies: statistics – galaxies: stellar content

1. INTRODUCTION

Given their large size (∼Mpc), mass ($\sim 10^{14}\ M_\odot$), and energetics ($>10^{64}$ erg in cluster–cluster mergers), galaxy clusters make excellent laboratories for a variety of extragalactic and cosmological studies (see, e.g., Voit 2005 for a review). Of particular interest to galaxy formation modeling is trying to understand the relative distribution and evolution of the three main contributors to cluster mass: the stars (primarily residing in galaxies), the hot intracluster medium, and the dark matter. The dominant dark matter and gas components are fairly well constrained by gravitational lensing (e.g., Kaiser et al. 1995; Allen 1998; Bartelmann & Schneider 2001; High et al. 2012; von der Linden et al. 2014a) and X-ray observations (White et al. 1997; Jones & Forman 1999; Mohr et al. 1999; Allen et al. 2002, 2004; Vikhlinin et al. 2006), respectively. However, the stellar mass, as traced by optical or near-IR emission, is often poorly determined, with typical uncertainties exceeding factors of two (see, e.g., Gonzalez et al. 2007, 2013; Courteau et al. 2014). Uncertain stellar mass-to-light (M^*/L) ratios, which reflect the nature of stellar populations in various galaxy environments and their dependencies on global cluster parameters, are the dominant source of error in stellar mass estimates. Additional uncertainty comes from the large extent of the central cluster galaxy which blends into the faint and diffuse intracluster light (e.g., Gonzalez et al. 2005; Kravtsov et al. 2014).

Precise mass accounting of the baryons and dark matter can provide constraints on cosmological parameters, under the assumption that the average cluster's composition should be representative of the cosmic proportions (e.g., White et al. 1993; Allen et al. 2002; Voit 2005). Thus, one expects the baryon fraction, $f_{\rm baryon} = (M^* + M_{\rm gas})/M_{\rm tot}$, as well as the stellar mass fraction, $f_\star = M^*/M_{\rm tot}$, to be common to clusters of all scales (Schneider 2006), and within ∼10% of the universal mean (e.g., Kravtsov et al. 2005). However, current estimates of the baryon fraction in galaxy clusters fall short of the universal mean $f_b = \Omega_b/\Omega_m \approx 0.15$ and 0.17 measured by Planck (Planck Collaboration et al. 2014) and *Wilkinson Microwave Anisotropy Probe* (*WMAP*; Dunkley et al. 2009; Komatsu et al. 2011) respectively, with multiple studies showing that the stellar fraction, $f_\star$, decreases with increasing cluster mass (e.g., Lin et al. 2003; Gonzalez et al. 2007, 2013; Giodini et al. 2009; Andreon 2010; Dai et al. 2010; Laganá et al. 2011; Zhang et al. 2011b; Lin et al. 2012; Leauthaud et al. 2012). Moreover, these authors find that the star-to-gas fraction is a strongly decreasing function of cluster mass (see Figure 10 in Gonzalez et al. 2013). The reliable interpretation of these trends relies critically on the accuracy and applicability of the adopted mass measures. Multiple examples of the so-called uniform-field approximation (White et al. 1993) whereby a single *constant* M^*/L ratio is used to compute the total stellar masses of galaxy clusters are found throughout the literature. In addition to failing to explicitly consider the variation in stellar and galactic populations within a cluster, the adopted M^*/L values are typically derived from studies of biased galaxy populations (e.g., often applicable to an old (∼10 Gyr) stellar population).

A standard approach to retrieving galaxy properties (including stellar masses) from spectra uses stellar population synthesis (SPS) modeling (Tinsley & Gunn 1976; Tinsley 1978; Bruzual 1983; Bruzual & Charlot 1993; Maraston 2005; Conroy 2013; Courteau et al. 2014). This approach involves synthesizing theoretical stellar spectra and fitting a library of ensemble scenarios to the observed galaxy spectra or spectral energy distribution (SED) in order to assign parameters of the best-fit population model to the physical galaxy (i.e., SED-fit). The standard ingredients of SPS are stellar evolution models (e.g., Bruzual & Charlot 2003; Maraston 2005) and an initial mass function (IMF; e.g., Salpeter 1955; Kroupa 2001; Chabrier 2003).

[4] Hubble Fellow.

The evolution of multiple, single stellar populations are superimposed over one another according to a prescribed set of stellar formation histories (SFHs; see Walcher et al. 2011, Conroy 2013, and Courteau et al. 2014 for recent reviews). The accuracy of the stellar population model typically improves as the spectral coverage increases, but so do the observational and computational expenses.

The relationship between color and $\log(M^*/L)$ (or "CMLR" for "color mass-to-light relations") has been determined for various widely used broadband filter combinations (e.g., Bell & de Jong 2001; Bell et al. 2003; Zibetti et al. 2009; Taylor et al. 2011; Into & Portinari 2013). While robust within their respective definitions, the scatter between these CMLRs is still large due to intrinsic sample variance, model degeneracies, observational limitations, and more. Systematic differences between CMLRs arise from implementing different stellar evolution models using a range of assumptions for, e.g., the IMF, SFH, and metallicity, as well as different SPS libraries, many of which are contentious (Courteau et al. 2014). Even with the highest quality multi-wavelength data, these various uncertainties cap the accuracy of CMLR stellar mass determinations at ∼0.1–0.3 dex (Gallazzi & Bell 2009; Conroy et al. 2009; Conroy & Gunn 2010; Behroozi et al. 2010). Other possible avenues to rapidly estimating M^*/L, such as relations between M^*/L and galaxy luminosity (or "LMLR" for "luminosity mass-to-light relations"), carry comparable uncertainties (e.g., van der Marel 1991; Bell et al. 2003; Kauffmann et al. 2003; Cappellari et al. 2006). Despite their limitations, these methods have gained popularity for their straightforward implementation over large galaxy samples.

For instance, the Cappellari et al. (2006) LMLR is the basis of the stellar mass estimates made by Gonzalez et al. (2007) and Andreon (2010). In Gonzalez et al. (2007), the variation in cluster galaxy population is taken to be encoded in the luminosity function (LF), which is itself uncertain. Integration over the cluster LF results in a luminosity-weighted $M^*/L_I = 3.6$. Andreon (2010) use an average value from Cappellari et al. (2006) of $M^*/L_I = 3.8$. However, as Leauthaud et al. (2012) point out, the SAURON sample upon which the Cappellari et al. (2006) LMLR is based comprises only early-type galaxies. A dynamical mass component, which includes contributions from dark matter, is also invoked in modeling their LMLR. Gonzalez et al. (2013) correct for the latter effect but still adopt a single, constant (albeit revised and more representative) mass-to-light ratio for all clusters ($M^*/L_I = 2.65$). Lin et al. (2003) employ a similar method, utilizing separate M^*/L_K's for ellipticals and spirals weighted by their respective K-band LFs. The final cluster M^*/L_K is an average of the two galaxy populations, weighted by the expected spiral fraction for that X-ray temperature (T_X). Other examples of recent stellar mass census that rely on mass-to-light ratios include Arnouts et al. (2007), Dai et al. (2010), Zhang et al. (2011b), and Lin et al. (2012). Leauthaud et al. (2012) caution against the use of constant M/L ratios in converting cluster luminosity into stellar masses, arguing that these are biased toward certain galaxy populations. Using a sample of galaxy groups in the COSMOS multi-waveband survey ($10^{13}\ M_\odot < M_{\rm halo} < 10^{14}\ M_\odot$), they showed that, if the stellar mass of each galaxy is computed independently, the total inferred $f_\star$ is significantly lower than that reported by previous works that assume a constant M^*/L. Leauthaud et al. (2012) attribute this discrepancy to a combination of the shortfall of the constant M^*/L approximation (with bias toward early-type galaxies, relevant for all mass retrieval methods) and systematic differences in SPS modeling.

Any single M/L ratio assumption inevitably fails to capture the full complexities of a cluster system. Indeed, Lin et al. (2012) note that a constant M^*/L ratio is robust only in the event of a weak dependence on stellar mass or morphology. In this work, we will assess the validity of the assumption of a constant M^*/L on cluster scales, and the effects of different SPS packages on the inferred cluster-wide value of M^*/L. To this end, we have assembled a sample of nearby clusters with available multi-band optical and X-ray data. We compile cluster stellar luminosities and masses on a galaxy-by-galaxy basis using our own membership assignment scheme. The stellar masses are evaluated using various color-based mass-to-light ratio transformations, as well as SED fits to broadband optical photometry, *for each galaxy in the cluster*. This analysis yields estimates for the total stellar content in these clusters (with limitations, as we will discuss below), as well as cluster-wide stellar mass-to-light ratios, whose variations among clusters is of special interest. This effectively extends the analysis by Leauthaud et al. (2012) to halos in the mass range $10^{14}\ M_\odot$–$10^{15}\ M_\odot$.

Our paper is organized as follows: the cluster sample and data source are described in Section 2 and our treatment of the cluster membership—a chief source of uncertainty in the absence of full spectroscopic coverage—is presented in Section 3. Stellar mass derivations and the convergence to our preferred approach are addressed in Section 4. Results and discussions are found in Section 5. Our main conclusions and a look toward future investigations are presented in Section 6.

Throughout this work, we adopt the ΛCDM cosmology with $H_0 = 71$ km s^{-1} Mpc^{-1}, $\Omega_M = 0.27$, and $\Omega_\Lambda = 0.73$.

2. SAMPLE AND DATA

2.1. Sample

Our proposed investigation requires reliable X-ray measurements, which constrain the total halo mass (assuming hydrostatic equilibrium), and multi-band optical photometry, which will facilitate the computation of galaxy stellar masses. We draw from three published X-ray studies of nearby galaxy clusters, all based on *Chandra* observations: Vikhlinin et al.'s (2006) first sample of nearby relaxed clusters, Vikhlinin et al.'s (2009) expanded sample as a follow-up to the *ROSAT* 400 deg^2 survey, and Sun et al.'s (2009) analysis of low-mass clusters and groups. We require that the selected clusters overlap with the Sloan Digital Sky Survey (SDSS) Data Release 10 (DR10; Ahn et al. 2014) which provides optical photometry (*u,g,r,i,z*) and spectroscopy for a flux-limited sample of galaxies within each cluster. We impose a redshift range of $0.04 < z < 0.1$ in order to exclude both very nearby clusters (e.g., Virgo), for which "shredding" of large galaxies is an issue, and distant clusters, for which SDSS fails to sample the cluster galaxy LF to sufficient depth. Additional selection criteria include dynamic relaxedness (based on visual inspection of X-ray morphology), availability of total mass estimates (M_{500} from X-ray spectroscopy, assuming hydrostatic equilibrium), and some spectroscopic coverage (to anchor bright cluster members).

The final sample of 12 clusters, tabulated in Table 1, spans a range in halo mass of 0.5–$12 \times 10^{14}\ M_\odot$. The virial mass estimates, M_{500}, are taken from the literature (see Table 1) and

Table 1
Properties of Galaxy Clusters in Our Sample

Cluster	R.A. (°)	Decl. (°)	z	M_{500} (10^{14} $M_{\odot}$)	Reference
A85	10.460	−9.303	0.0557	5.98	1
A160	18.248	15.491	0.0447	0.79	3
A1650	194.673	−1.761	0.0823	4.59	1
A1692	198.057	−0.974	0.0848	0.970	3
A1795	207.217	26.591	0.0622	5.46	1
A1991	223.631	18.642	0.0592	1.23	2
A2029	227.734	5.745	0.0779	8.01	2
A2142	239.583	27.233	0.0904	11.96	1
A2244	255.677	34.060	0.0989	5.11	1
MKW 3s	230.466	7.709	0.0453	2.09	1
UGC 842	19.723	−1.002	0.0452	0.560	3
Zw1215	184.421	3.656	0.0767	5.75	1

References. (1) Vikhlinin et al. (2006); (2) Vikhlinin et al. (2009); (3) Sun et al. (2009).

represent the total mass enclosed within the radius R_{500}.[5] Given M_{500} and $\rho_{\rm crit}$ at the cluster redshift, R_{500} can be computed from:

$$R_{500} = \left(\frac{3}{4\pi}\frac{M_{500}}{500\rho_{\rm crit}}\right)^{1/3}. \quad (1)$$

2.2. Data

Optical photometry and, where possible, spectroscopic redshifts, are obtained from SDSS DR10 for all galaxies in each cluster that lie within an angular separation corresponding to R_{500} on the sky. Throughout this work we utilize SDSS's "composite model magnitudes" (cmodelMag), which represent a linear combination of the best-fit exponential and $r^{1/4}$ (de Vaucouleurs 1948) models to the galaxy surface brightness profile (Stoughton et al. 2002).

We caution that SDSS model magnitudes and sizes may still be subject to systematic errors, such as deprojection effects (e.g., Hall et al. 2012), a detailed investigation of which is beyond the scope of the present study. Notably, several recent studies (e.g., Bernardi et al. 2013, and references therein) have shown that SDSS model photometry underpredicts luminosity from the brightest galaxies. We do not expect our conclusions to be affected by such a deficiency in the overall stellar content, assuming that the stellar populations (specifically the stellar mass-to-light ratio) do not vary in the galaxies' outskirts (which we may be missing). Based on a careful re-analysis of SDSS imaging for Virgo cluster galaxies, Roediger et al. (2011) find that the stellar populations gradients at large galactocentric radii are flat. Nevertheless, we present an analysis of possible photometric biases and their effect on our study in Section 5.3. Galactic extinction estimates for each galaxy are obtained from SDSS and are used to compute extinction-corrected fluxes. K-correction terms provided by SDSS will be used for CMLR-based stellar mass estimates (see Section 4).

3. METHODOLOGY

We now describe the method by which the total luminosity and stellar mass for each cluster are derived.

In order to accurately measure the total luminosity and stellar mass for a given galaxy cluster, the identification of all cluster galaxies is crucial. Ideally, we wish to maximize completeness in cluster member detections while minimizing contamination from foreground and/or background galaxies due to projection. Traditionally, cluster-searching algorithms have been plagued by the trade-off between these two requirements. Whereas the most conservative membership algorithm, which only considers spectroscopically confirmed galaxies, achieves minimal contamination, it is observationally expensive and requires pre-selection of spectroscopic targets which may be biased toward bright, red-sequence galaxies.

Conversely, purely photometric membership assessment (e.g., selection by color through red-sequence identifications or by a luminosity cut) assume a strict uniformity in the galaxy population and can miss blue cluster members (i.e., incompleteness), or incorrectly include field galaxies with fortuitous colors that match the cluster's average (i.e., contamination). Photometric redshifts, typically based on SED-fitting (see, e.g., Bolzonella et al. 2000) allow for more robust rejection of foreground/background contamination; however, the achieved precision is not sufficient for definitive individual member assignments. As a compromise, we employ spectroscopic redshifts where available (see Table 3) and utilize photometric redshifts as distance indicators in a statistical sense in order to reject foreground and background galaxy populations without imparting a color bias on our galaxy sample.

We require that all identified galaxies be detected in both binned and unbinned data, be appropriately treated for blending, and have no major photometric issues.[6] We adopt a brightness limit of $r < 22$, below which SDSS is generally incomplete, and require that all galaxies lie within a distance of R_{500} from the BCG.

We use photometric redshifts ($z_{\rm phot}$) from the photo-z table in the SDSS3 DR10 which is defined for all galaxies with reliable photometry in the survey. These are derived from five-band photometry using a KD-tree nearest neighbor fit (KF), as described in Csabai et al. (2007). The alternative $z_{\rm phot}$ catalog in DR10 (PhotozRF) uses random forests to determine these values (Carliles et al. 2010). Since the two techniques yield similar accuracy and statistical properties (see Figure 1), we use the former, which also contains the quality assurance parameter $nnCount$ to indicate the extent of the spectroscopic training set coverage. K-correction in each waveband is deduced via SED template fitting as part of DR10.

For each cluster in our sample, we generate 1000 realizations, each containing a subset of all galaxies found within the projected R_{500}. The likelihood of a galaxy being included in any given cluster realization depends on the probability of its measured z falling within the cluster range, taken to be $z_{\rm clust} \pm \delta z$, where δz encompasses the expected velocity dispersion for a given cluster characteristic radius. σ_v is related to R_{500} via the relation from Zhang et al. 2011a:

$$\log\left(\frac{R_{500}}{\rm kpc}\right) = 3.07 + 0.89\log\left(\frac{\sigma_v}{1000\ {\rm km\ s^{-1}}}\right). \quad (2)$$

We approximate the acceptable range of redshifts for galaxies bound to the cluster as $\delta z \approx dv/c = 2\sigma_v/c$, thus allowing

[5] r_Δ is the radius within which the mean enclosed density is $\Delta * \rho_{\rm crit}$, provisionally defining the outer boundary of a cluster.

[6] SDSS parameters are used to perform photometric quality checks and derive fluxes as follows: for each galaxy to be considered, cmodelMag must be defined within each band, and z-phot must exist. We demand that "other" flags not be present to maintain the photometric integrity of our galaxies, except where possibly the BCG or a spectroscopically confirmed member is involved. These "other" flags are, following Szabo et al. 2011: TOO_FEW_GOOD_DETECTIONS, NOTCHECKED_CENTER, NOPROFILE, and BADSKY.

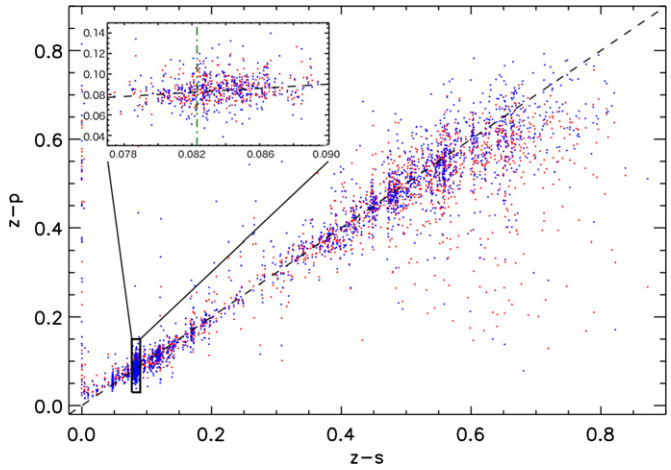

Figure 1. Comparison between $z_{\rm phot}$ (z–p) as deduced by methods KF (blue dots) and RF (red dots), vs. $z_{\rm spec}$ (z–s), for galaxies with SDSS spectroscopy around the position of A1650. The dashed diagonal represents equality between $z_{\rm phot}$ and $z_{\rm spec}$. The inset magnifies the heavily populated region around the cluster redshift. Overall, KF and RF photometric redshifts have similar accuracy and scatter properties, especially over the redshift range of relevance for this study.

Table 2
Estimated Metrics for the Cluster Sample

Cluster	z	δz[a]	M_{500} ($10^{14}\ M_\odot$)	M_{200}[b] ($10^{14}\ M_\odot$)	r_{500} (Mpc)	r_{200}[b] (Mpc)
A85	0.0557	0.007	5.98	11.49	1.249	2.11
A160	0.0447	0.003	0.79	1.43	0.626	1.05
A1650	0.0823	0.006	4.59	8.58	1.135	1.90
A1692	0.0848	0.003	0.970	1.72	0.658	1.11
A1795	0.0622	0.007	5.46	10.41	1.235	2.04
A1991	0.0592	0.004	1.23	2.23	0.732	1.23
A2029	0.0779	0.008	8.01	15.3	1.362	2.31
A2142	0.0904	0.009	11.96	23.03	1.558	2.63
A2244	0.0989	0.007	5.11	9.49	1.170	1.95
MKW 3s	0.0453	0.005	2.09	3.89	0.882	1.47
UGC 842	0.0452	0.003	0.560	0.99	0.570	9.36
Zw1215	0.0767	0.007	5.75	10.88	1.225	2.06

Notes.
[a] Velocity width of cluster from Zhang et al. (2011b).
[b] Assumes NFW dark matter halo (Duffy et al. 2008).

galaxies with line-of-sight velocities within $dv = 2\sigma_v$ of the cluster center. Column 3 of Table 2 provides δz for each cluster.

The adoption of a radial velocity interval bracketing the cluster's cosmological redshift as a criterion for assigning cluster membership differs from exclusively selecting galaxies located within the sphere of radius R_{500} around the cluster center. In particular, infalling galaxies outside the nominal cluster search radius, as well as foreground/background galaxies, could spoil this operation. We assess these effects below using simulated clusters from the Millennium Simulation (Springel et al. 2005).

Assuming that the probability distributions for both $z_{\rm phot}$ and $z_{\rm spec}$ are Gaussian, with widths given by the quoted redshift uncertainty ($z_{\rm err}$), the probability that a given galaxy belongs in the cluster can be:

$$P(\text{member}) = \int_{z_{cl}-\delta z}^{z_{cl}+\delta z} \frac{1}{\sqrt{2\pi}\, z_{\rm err}} \exp\left(-\frac{(z - z_{\rm gal})^2}{2 z_{\rm err}^2}\right) dz. \quad (3)$$

In practice, a random $z_{\rm gal}$ value is drawn from the Gaussian distribution as in the integrand of Equation (3) and compared to $z_{\rm clust}$. If it falls within the interval $z_{\rm clust} \pm \delta z$, then it is accepted. Otherwise, it is excluded from any particular cluster realization. A library of 1000 such realizations is produced for each cluster, thus statistically accounting for the membership uncertainty due to uncertainty in distance. This action offsets contamination while still considering every galaxy detected within the projected cluster radius. The distributions of luminosity, mass, and M^*/L for the 1000 realizations provide the relevant uncertainty estimates. Given the order-of-magnitude precision improvement on spectroscopic redshifts, clusters with many spectroscopically confirmed members will naturally have more tightly constrained measurements. The number of photometrically and spectroscopically confirmed galaxies in each cluster is summarized in Table 3.

Table 3
Number of Galaxies Detected in Each Cluster

Cluster	$N_{\rm gal}^{\rm tot}$ ($r < R_{500}$)	w/spec	$N_{\rm gal}^{\rm spec}$	$N_{\rm gal}^{\rm boot}$
A85	2640	140	87	167
A160	856	67	33	34
A1650	1183	64	28	79
A1692	303	20	16	19
A1795	2408	145	82	144
A1991	1086	70	35	51
A2029	1809	149	94	173
A2142	2195	193	102	254
A2244	1226	91	48	108
MKW 3s	1627	97	45	68
UGC 842	652	65	26	29
Zw1215	1330	127	66	141

Notes. $N_{\rm gal}^{\rm tot}$: number of photometrically detected galaxies within R_{500}. $N_{\rm gal}^{\rm spec}$: number of spectroscopically confirmed cluster galaxies. $N_{\rm gal}^{\rm boot}$: median number of cluster galaxies from bootstrap analysis.

To assess the robustness of our $z_{\rm phot}$-based cluster construction scheme, we perform several sanity checks. For one, we can compare our measured mass–richness relation with previous works. Andreon & Hurn (2010), who define richness (N_{200}) as the number of bright ($M_V < -20$) red galaxies within R_{200}, find:

$$\log\left(\frac{M_{200}}{M_\odot}\right) = (0.96 \pm 0.15)(\log(N_{200}) - 1.5) + (14.36 \pm 0.04), \quad (4)$$

from a fit to 53 cluster caustic masses in a Bayesian framework. Note the Andreon & Hurn study only involves clusters with $M_{200} \lesssim 10^{15}\ M_\odot$ (see their Figure 2).

To ensure a fair comparison, we first convert from R_{500}, M_{500} to R_{200}, M_{200} assuming a Navarro–Frenk–White (NFW) profile for the cluster halo distribution, following Duffy et al. (2008; see Table 2). Adopting R_{200} also modifies the search radius around each cluster for member galaxies, requiring us to re-run the cluster-construction bootstrap analysis after first discarding all galaxies that fall below the $M_V < -20$ brightness criterion of Andreon & Hurn (2010; assuming $V = g - 0.5784(g - r) - 0.0038$; Lupton et al. 2005).

Figure 2 summarizes the results of this comparison. Our cluster points, built from the described $z_{\rm phot}$-PDF based member selection described above, agree well with both the slope and scatter quoted by Andreon & Hurn (2010) in the lower cluster mass ranges (i.e., $\lesssim 10^{15}\ M_\odot$) where the two samples overlap. At $\gtrsim 10^{15}\ M_\odot$, we find systematically lower values of N_{200} compared to Andreon & Hurn (2010), though the two

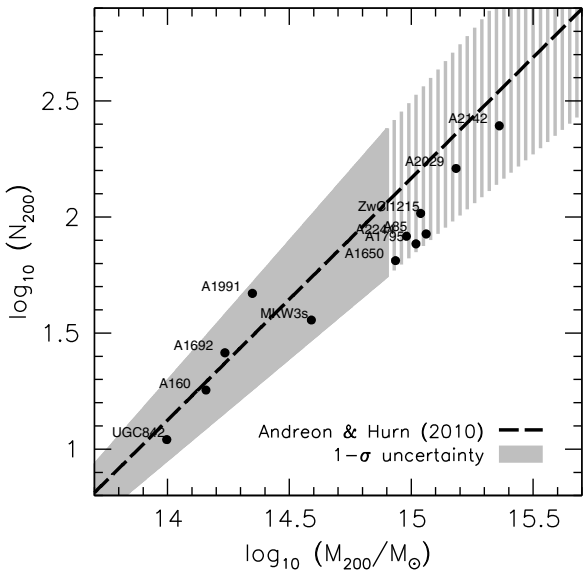

Figure 2. Comparison between the M_{200} and N_{200} scaling relation of Andreon & Hurn (2010) and that from our $z_{\rm phot}$-based Monte Carlo cluster construction. The shaded area represents the combined 1σ slope uncertainty and scatter quoted by Andreon and Hurn. Note that this relation is only well-constrained for $13.7 < \log_{10} M_{200} < 14.9$—we have highlighted the fact that we are showing an extrapolation by using a hashed fill for $\log_{10} M_{200} > 14.9$.

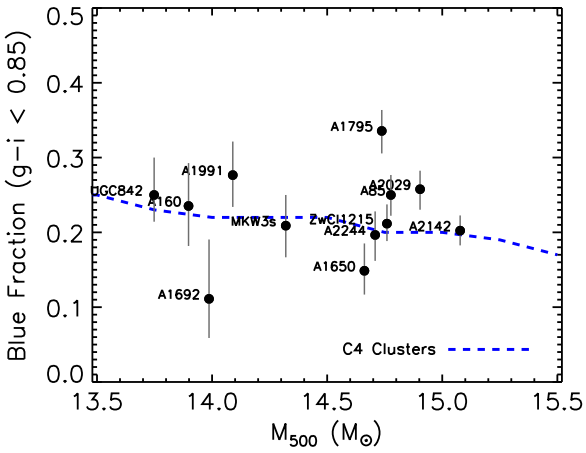

Figure 3. Comparison of the fraction of blue galaxies (with $g - i < 0.85$) from our analysis to the typical cluster spiral fraction as a function of halo mass. The dashed line follows the occurrence of spiral galaxies in the C4 Clusters sample (Miller et al. 2005) as detected by Hoyle et al. (2012) via use of the Galaxy Zoo project. While C4's downward trend is not apparently replicated by our (limited) sample, the overall agreement is satisfactory given the large uncertainties in both measurements.

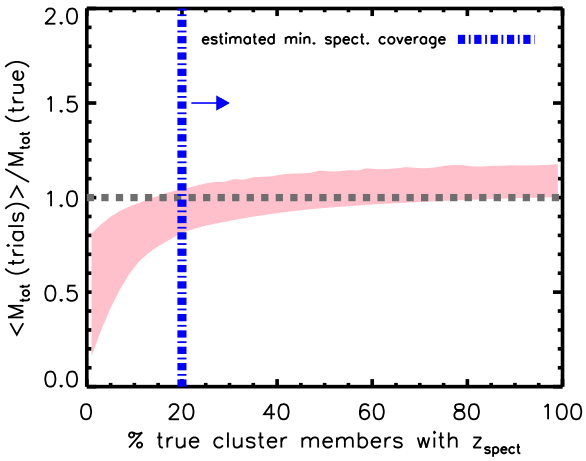

Figure 4. Demonstration of the accuracy of aggregate mass estimates from the zphot bootstrap method described in Section 3, using galaxy clusters in the Millennium Simulation where the "true" mass is known. The probabilistic total mass in galaxy halos obtained from cluster realizations is compared with the (fixed and known) total mass in true members. The shaded region spans the range of outcomes corresponding to each cluster/orientation combination. See text for more details about the simulations. For clusters with >20% spectroscopic member confirmation—satisfied for all the clusters in this study—the derived halo masses are at most 20% (typically <10%) discrepant from their true value.

samples still agree within the 1σ uncertainties (see shaded region in Figure 2). We measure a slightly shallower slope to the N_{200}–M_{200} relation of 0.82 ± 0.08, consistent at the 1σ level with the value of 1.04 ± 0.16 quoted by Andreon & Hurn (2010).

We further examine whether the measured fractions of blue galaxies in the clusters are realistic. Blue galaxies are defined here as having extinction-corrected $g - i < 0.85$. Figure 3 illustrates, as a function of M_{500}, the median and 1σ fraction of blue galaxies with respect to total number of cluster members over 1000 realizations. Overplotted are results from measurements of spiral fractions in the C4 cluster catalog (Miller et al. 2005) by Hoyle et al. (2012). Although the two metrics are not identical, they are expected to be similar. Our measured blue fractions (∼20%–30%) are consistent with the expected spiral fraction in massive clusters ($10^{13.5}\ M_\odot < M_{500} < 10^{15}\ M_\odot$), further validating our method.

As another important check, we gauge the discrepancy between the actual aggregate mass (i.e., from all true cluster members within the spherical volume defined by R_{500}) and that inferred by our $z_{\rm phot}$ probabilistic scheme. We do this using simulated clusters and field galaxy halos from the Millennium Simulation (Springel et al. 2005). We choose two group-sized halos (∼50 members) and two cluster-sized halos (∼300 members) at $z \sim 0.06$. These structures are identified using a friends-of-friends algorithm. Individual galaxy properties, including stellar mass, for each subhalo are provided by De Lucia et al. (2006). For each group/cluster, we extract three-dimensional positions and stellar masses for all galaxies within $R_{200,\rm crit}$ and with $M_* > 10^9\ M_\odot$ (roughly mimicking our sensitivity limit), projecting the cluster on the sky along three different axes for each cluster (probing different line-of-sight structure). For each cluster and line-of-sight orientation, we obtain the true redshift of every galaxy halo within the cylinder of $R_{200,\rm crit}$ (converting line-of-sight distance to radial velocity) and assign to them a characteristic photometric redshift uncertainty $dz_{\rm phot} = 0.03$. This choice is motivated by typical errors on $z_{\rm phot}$ as reported in the SDSS photo-z table for galaxies at $z = 0$–0.2 (see also Figure 1). For a subset of the true cluster members we also assign spectroscopic redshifts—that is, probability density functions (PDFs) which have negligible error centered on the true z—in order to quantify the effects of spectroscopic incompleteness.

We then perform a bootstrap analysis following the procedure described above (assuming a Gaussian PDF with width $dz_{\rm phot} = 0.03$ for $z_{\rm phot}$) to build cluster realizations, and tabulate the resultant total stellar masses. As a function of the fractional spectroscopic coverage for true cluster members (assuming more massive cluster member are prioritized in spectra acquisition, which is typically the case for SDSS), the statistically inferred and true masses are, on average, within 20% of one another once we have at least 10% spectroscopic confirmation (Figure 4). While we do not know the "true" number of galaxies within a three-dimensional radius for the clusters in our sample, we estimate from richness-halo mass relations—calibrated

on well-studied, low-redshift clusters (Andreon & Hurn 2010; High et al. 2010)—that our typical spectroscopic completeness is >20% for the systems analyzed in this study.

Figure 4 illustrates the bias in the total stellar mass for the 12 cluster-line-of-sight combinations simulated. Not surprisingly, sparse spectroscopic coverage can cause significant downward bias in the inferred mass metric for the cluster, due to cluster members with large redshift uncertainties scattering out of the cluster volume. Fortunately, in this regime the marginal rate of improvement with spectroscopic redshifts is also high. Again, if $z_{\rm spect}$ is available for 10% or more of the most prominent cluster galaxies, the typical error on galaxy mass derived from our method is less than 20%. Note that this discrepancy incorporates contributions from the distinction between cylinder and sphere in our three-dimensional volume selection. The positive bias in the regime of high-completeness spectroscopic coverage is due to contamination of foreground/background galaxies and the geometric factor between spherical and cylindrical volume selection. This bias can be reduced with some spectroscopic coverage of the field population, potentially excluding heavyweight contaminants. While such $z_{\rm spect}$ for field galaxies is not considered in the present test, it has been used for membership exclusion in the analysis of our sample. This implies a ∼10% uncertainty on the true stellar mass for systems studied in this paper, which is less than the uncertainty in the X-ray-derived total cluster mass.

The measurement of the blue fraction will be similarly biased. Using the same techniques outlined above, we find that the blue fraction will be biased high by ∼8% for typical clusters in our sample, due to field galaxies lying along the line of sight. This bias is small—our typical measurement uncertainty is ∼5%–10%—though it may be large enough to wash out any subtle trends with blue fraction, since the overall range in blue fraction only spans ∼25% in this sample (see Figure 3).

We caution that the scheme thus far outlined has obvious limitations. First, the aforementioned probabilistic treatment of galaxy membership, as in Equation (3), is oversimplified. Ideally, one would marginalize over the precise $z_{\rm phot}$ PDFs in favor of the fiducial Gaussian form employed here. Such avenues are beyond the scope of the current paper. Second, our Monte Carlo method is naturally biased to galaxies with spectroscopic redshifts. Spectroscopic redshifts have very sharply peaked PDFs with error widths of $\sim 10^{-4}$, and thus tend to be included in either 0% or 100% of the cluster realizations. In the test above, we have demonstrated the importance of at least modest spectroscopic coverage in securing the validity of our methodology, but with a specific assumption about the availability of spectra as a function of cluster member properties (i.e., preference is given to more massive galaxies). In reality, whether a galaxy is part of a spectroscopic target program is somewhat arbitrary (although spectroscopic coverage is certainly skewed toward the brightest members), leading to a somewhat asymmetric selection bias which entails a greater uncertainty than is captured in the PDFs alone.

Other errors inherent to our cluster galaxy stellar mass accounting technique include incompleteness due to the magnitude-limited nature of the survey sample, as well as deprojection effects due to the selection of galaxies within a redshift cylinder as opposed to a sphere. The former problem biases our resultant total stellar mass low, while the latter overestimates the total number of galaxies in each cluster. A correction factor could be applied to compensate for each effect as gauged by, e.g., mock catalogs. A similar treatment by Leauthaud et al. (2012) for COSMOS galaxy groups yielded a correction factor <15% which is estimated to be much less than systematic errors in the stellar mass estimates themselves (Section 5). Such a correction is also consistent with Figure 4. As described above, we find from halo-only simulations that the mass bias due to selection on radial velocity (rather than a three-dimensional cut) is ∼10% for a wide range in cluster masses. We therefore ignore this effect for the present study. As long as the faintest, low-mass systems, as well as those residing in the space between the sphere and its cylindrical counterpart are not strongly skewing the M^*/L distribution, then the measured M^*/L should be representative of the true value. We briefly return to this point in Section 5.4.

Table 4
Coefficients for the Relation $\log_{10}(M*/L_\lambda) = a_{\lambda,\rm col} + (b_{\lambda,\rm col} * col)$

Reference	$a_{i,g-i}$	$b_{i,g-i}$
Bell et al. (2003) diet Salpeter	−0.152	0.518
Bell et al. (2003) Kroupa or Kennicutt	−0.302	0.518
Zibetti et al. (2009)	−0.963	1.032
Taylor et al. (2011)	−0.68	0.70
Into & Portinari (2013)	−0.625	0.897

4. STELLAR MASS ESTIMATION

As discussed in Section 2.2, stellar masses of galaxies are popularly inferred from photometry via simple color–M^*/L (CMLR; fast, but with large uncertainties), or full-scale SED-fitting (more reliable but expensive) on which the CMLRs are based. Below we explore both of these approaches, providing multiple estimates of stellar mass for each cluster and allowing us to assess the similarities and differences of each formalism.

4.1. Stellar Masses via Color–M^*/L Transformations

Numerous CMLRs are now available, some based purely on stellar evolution model libraries (e.g., Zibetti et al. 2009, hereafter Zi09; Into & Portinari 2013, hereafter Ip13)), and others depending on a subset of these libraries constrained by observation (e.g., Bell et al. 2003, hereafter Be03; Taylor et al. 2011, hereafter Ta11). These relations are generically expressed as:

$$\log_{10}\left(\frac{M^*}{L_\lambda}\right) = a_{\lambda,\rm color} + (b_{\lambda,\rm color} \times \rm color), \quad (5)$$

where $a_{\lambda,\rm colour}$ and $b_{\lambda,\rm colour}$ are the normalization and slope, respectively, for a given relation. Each of the aforementioned papers provide waveband- and color-dependent $a_{\lambda,\rm colour}$ and $b_{\lambda,\rm colour}$ terms, which we summarize in Table 4. The amount of scatter in a given CMLR relation varies with both the luminosity band and color chosen. For this work, we adopt the i-band luminosity with the $g-i$ color due to their higher signal-to-noise ratio over other SDSS bands, broad baseline, and stable CMLR (Taylor et al. 2011).

The variance in the slope and the normalization of these relations highlights large systematic differences between the relations. In general, the large differences in $a_{i,g-i}$ from Table 4 arise from different choices of IMF between authors. Further discrepancies in both $a_{i,g-i}$ and $b_{i,g-i}$ between authors arise from a variety of assumptions implicit in the stellar population libraries (SPL), including details of stellar evolution models (e.g., asymptotic giant branch (AGB) modeling), star formation history, and treatment of dust extinction. Each CMLR also

Table 5
Properties of Various Stellar Population Models from the Literature

References	SPS	IMF	SFH	Metallicity	Dust	Test Data Set
Be03	PÉGASE[a]	diet Salpeter[b] Kroupa or Kennicutt[e]	exponential SFR[c]	···	n/a	SDSS EDR[d]
Zi09	CB07[f]	Chabrier[g]	exponential + bursts	0.2 to 2 solar	CF00[h]	n/a
Ta11	BC03[i]	Chabrier	exponential	0.005 to 2.5 solar	Calzetti[j]	GAMA[k]
Ip13	Padova isochrones[l]	Kroupa	exponential + b-parameter[m]	0.2 to 1.5 solar	n/a	n/a
MAGPHYS	CB07	Chabrier	exponential + bursts	solar	···	n/a

Notes.
[a] PÉGASE models (Fioc & Rocca-Volmerange 1997).
[b] Diet Salpeter IMF (Bell & de Jong 2001).
[c] Generically, SFR(t) $\propto e^{-t/\tau}$.
[d] Early Data Release (Stoughton et al. 2002).
[e] Kroupa (2001) or Kennicutt (1983) IMF.
[f] CB07 SPS codes (Bruzual 2007).
[g] Chabrier IMF (Chabrier 2003).
[h] An angle-averaged model (Charlot & Fall 2000).
[i] BC03 SPS codes (Bruzual & Charlot 2003).
[j] Calzetti dust obscuration law (Calzetti et al. 2000).
[k] Driver et al. (2009).
[l] Padova isochrones with TB-AGB treatment (Mariago & Girardi 2007).
[m] Birthrate = $\psi(T_{\rm present})/\langle\psi\rangle$ (Into & Portinari 2013).
[n] Dust around AGB stars.

depends on the empirical training data set used to refine the relations. Table 5 summarizes some of these model assumptions for several popular CMLRs. For a recent review of color diagnostics for galaxy M^*/L's, see Courteau et al. (2014).

For each individual galaxy, we use i-band luminosities and $g-i$ colors, corrected for Galactic extinction and k-corrected to $z = 0$, to arrive at an M^*/L using the various CMLRs described in Table 4. Stellar masses are computed via:

$$M^* = L_\lambda \times (M^*/L_\lambda), \quad (6)$$

where L_λ is the i-band luminosity.

4.2. Stellar Masses via SED Fitting with MAGPHYS

Although time-consuming and somewhat model dependent, SED fitting should provide more robust estimates of individual galaxy properties, due to its reliance on all five photometric bands (u, g, r, i, z), rather than only two (g, i). We use the publicly available software Multi-wavelength Analysis of Galaxy Physical Properties (MAGPHYS), a FORTRAN77 program developed by da Cunha et al. (2008), for our analysis. The SPL in MAGPHYS is constructed from the 2007 version of the Bruzual and Charlot (BC03, CB07) SPS code (Bruzual & Charlot 2003; Bruzual 2007), which contains an improved treatment of TB-AGB stars. A Chabrier IMF (Chabrier 2003) is assumed and dust attenuation follows the Charlot & Fall (2000) model. A wide range of SFHs are considered, and the parameter space is surveyed based on the notion that any SFH can be dissected into an underlying continuum of exponentially declining star formation rate (SFR) and a series of bursts (e.g., Kauffmann et al. 2003).

MAGPHYS requires a galaxy redshift ($z_{\rm gal}$) and the specific flux with its error (f_λ, df_λ) in each filter. The fluxes are corrected for Galactic extinction but not k-corrected since the program assembles its SPL at the galaxy's given redshift, effectively performing its own k-correction. All galaxies that are associated with the cluster for a given realization (see Section 3) are assigned the same redshift—this may introduce small systematic effects on a galaxy-by-galaxy basis, but these should disappear for the ensemble if the cluster is assumed to be symmetric along the line of sight. MAGPHYS outputs the stellar mass PDF for which we report the median value. The error range is indicated by the mass interval between the 16th and 84th percentile.

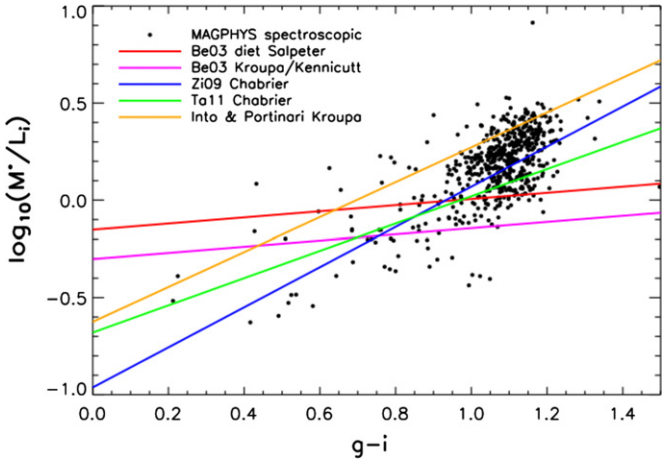

Figure 5. M^*/L_i vs. ($g-i$) color for various CMLRs and the MAGPHYS fits to u, g, r, i, z photometry for our spectroscopic subsample (black dots). The spectroscopic sample is preferentially selected for redder (usually brighter) galaxies, so little constraint is placed on the faint/blue regime. Stellar masses derived from SED-fits are matched by the Zi09, Ta11, and Ip13 formalisms and are most consistent with Zi09. Indeed, the underlying model assumptions upon which the Zi09 and MAGPHYS formalism are based (Table 5) share similarities. Bell et al. (2003), which assumes either a diet Salpeter or Kroupa IMF, predicts systematically higher stellar mass for bluer galaxies, and lower mass for redder galaxies.

The intrinsic discrepancies between various CMLRs and MAGPHYS are illustrated in Figure 5. The formulations from Bell et al. (2003) appear least consistent with the MAGPHYS data and competing formalisms. MAGPHYS-derived values are reasonably well matched by the other CMLRs (Zibetti et al. 2009; Taylor et al. 2011; Into & Portinari 2013).

4.3. Boostrapping Aggregation

We wish to consider the contribution of individual member galaxies to the total stellar mass-to-light ratio. In aggregating the observed luminosity and stellar mass over the detected galaxies, three sources of uncertainty should be explicitly addressed: (1) the measured luminosity (i.e., L-variance), (2) the light-to-mass conversion (i.e., M^*-variance), and (3) the membership assessment (i.e., cluster composition variance).

One approach to this problem involves bootstraping over reasonable PDFs for each quantity, on a galaxy-by-galaxy basis and for each cluster realization, as outlined in Section 3. Over a large number of simulations, PDFs for total L, M^*, and M^*/L may be generated and total errors attributable to the aforementioned uncertainty sources are encapsulated in the shapes of these final PDFs.

To this end, we draw, for each member galaxy in a given cluster realization, a random i-band luminosity from a Gaussian PDF centered on the extinction-corrected absolute magnitude, with variance as their respective uncertainties. For the CMLR mass conversion, this procedure is repeated for g-band luminosity to secure $g-i$. The chosen i-luminosity and $g-i$ color then yield a best-estimate of $\log_{10}(M^*/L_i)$ (i.e., Equation (5)) and Table 4). Another round of bootstrapping is performed whereby a $\log_{10}(M^*/L_i)$ is drawn from a Gaussian distribution with centroid at the best estimate and variance 0.1 dex, which represents the typical uncertainty in the CMLR. Finally, the galaxy's M^* is derived in accordance with Equation (6) *for this particular realization*.

With MAGPHYS, no color or direct evaluation of M^*/L_i is involved. Instead, we draw the stellar mass for each galaxy directly from the relevant PDF output by the program, again approximated to be Gaussian.

For galaxies whose measurement errors on m_i or m_g exceed 0.2, the photometry is deemed unreliable for robust CMLR applications. In such cases ($\lesssim$20% of all candidate galaxies), the stellar mass PDFs are replaced with MAGPHYS values, which takes multiband information and their respective errors into account.

This process is repeated for 1000 realizations, yielding well-sampled PDFs for M^*/L_i and M^* for each cluster which fully account for our uncertainty in cluster membership, optical photometry, and light-to-mass conversions.

5. RESULTS AND DISCUSSION

For each CMLR (or SED-fit), stellar mass-to-light ratios, stellar masses, and stellar mass fractions (relative to M_{500}) are extracted from each cluster PDF and compared with cluster luminosity, total halo mass (M_{500}), and blue fraction. In this section, we analyze these parameters, compare them with past studies, and interpret them in the context of cluster evolution theories.

5.1. Stellar Mass-to-light and Stellar Mass Fraction versus i-band Luminosity, M_{500}, and Blue Fraction

In Figure 6, we show the cluster-wide M^*/L_i as a function of i-band luminosity (L_i), halo mass within R_{500} (M_{500}), and blue fraction. Systematic vertical offsets and slope discrepancies in M^*/L_i can be attributed to differences in the applied luminosity-to-mass conversion schemes (more on those below). Note also that the overall trends (or lack thereof) across the different formalisms (CMLR versus SED-fitting, varying IMF, varying SPS) are qualitatively consistent. The values of M^*/L_i, L_i, and blue fraction correspond to the medians of their respective Monte Carlo distributions. The error ranges are taken to be between the 16th and 84th percentiles of these distributions.

Table 6
Variations in Cluster M_*/L_i for Various Models

Reference	M_*/L_i
Zibetti et al. (2009)	1.6 ± 0.2
Taylor et al. (2011)	1.3 ± 0.1
Into & Portinari (2013)	2.4 ± 0.3
MAGPHYS	1.6 ± 0.1

Table 6 summarizes the variation in cluster M^*/L_i for each CMLR and SED fit. While the M^*/L_i values span a broad range whose mean and width are contingent on the light-to-mass conversion used, there is little evidence that this variation varies with cluster luminosity (Pearson $R = -0.05$) or halo mass ($R = -0.09$). When the data are organized against blue fraction, a weak, declining trend of M^*/L_i with increasing blue fraction appears in both CMLR-based and SED-fitted outcomes ($R = -0.53$), as is expected, since "red" galaxies have more mass per unit red light.

In their Figure 7, Leauthaud et al. (2012) plot histograms of M^*/L_{i+} for a sample of low-z galaxy group members in the COSMOS survey, whose stellar masses were also derived from SED-fitting. The imaging (Cousins-i+ and Sloan i) is similar, and the Chabier IMF calibration is directly comparable to our MAGPHYS results. Therefore, we use their peak and variance of the M^*/L_{i+} distribution to construct a "COSMOS" data point for comparison. That point is shown in the bottom row of Figure 6, where the published COSMOS data effectively extend our work into the regime of lower mass and bluer systems.

Figure 6 (lower panels) shows the linear fits to the MAGPHYS-derived M^*/L_i as a function of cluster mass (M_{500}) and blue fraction, including the COSMOS data point described above. These fits were performed using a bootstrapped (100 realizations) bisector method (Akritas & Bershady 1996) which accounts for uncertainties in both observables, covariances between the observables, and intrinsic scatter. This method yields the following relations:

$$\frac{M^*}{L_i} = -(2.10 \pm 2.01) f_{\rm blue} + (2.17 \pm 0.45), \quad (7)$$

and

$$\frac{M^*}{L_i} = (-0.06 \pm 0.48) \log_{10}\left(\frac{M_{500}}{10^{14}\, M_\odot}\right) + (1.71 \pm 0.23), \quad (8)$$

with standard deviations of 0.20 and 0.21, respectively. While there is a weak trend toward decreasing M^*/L_i with increasing blue fraction in Figure 6, that trend is not statistically significant (Equation (7)). Further analysis of both rich clusters ($f_{\rm blue} < 0.1$) and poor groups ($f_{\rm blue} > 0.5$) could further constrain the relationship between the blue fraction and the global M^*/L_i, which ought to have a negative slope given that blue galaxies have lower M^*/L_i than red galaxies.

5.2. Variations due to L–M* Conversion Prescription

As demonstrated in Figures 6, the derived M^*/L_i's over the cluster mass range considered differ primarily between methodologies in zero-point and secondarily in scatter. The offsets range from Ta11 at the low end ($M^*/L_i \sim 1.3 \pm 0.1$),

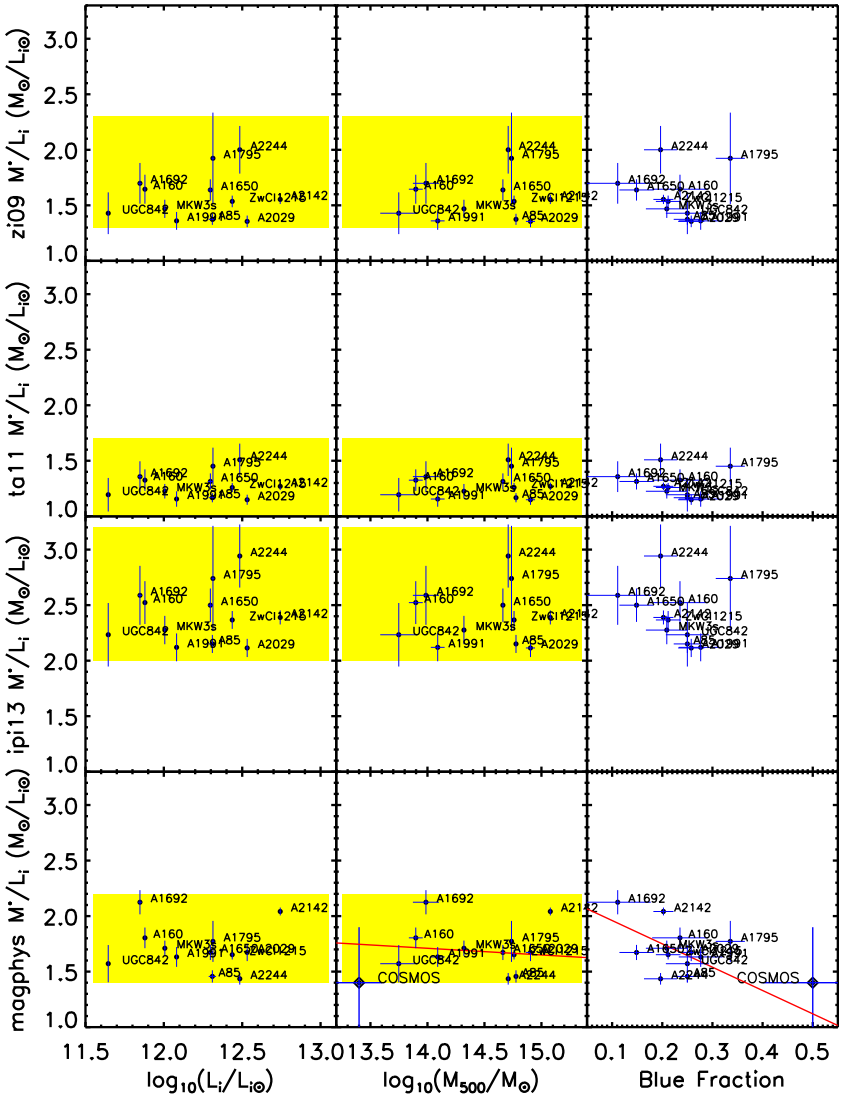

Figure 6. M^*/L_i vs. L_i, M_{500}, and blue fraction for our cluster sample. Shaded regions encompass the range of cluster stellar mass-to-light ratios specific to each stellar mass conversion method. The various methods yield results that are vertically offset from one another. A statistical analysis shows no significant correlation between M^*/L_i and the total mass (M_{500}) or blue fraction of the cluster galaxy population. Error bars are the statistical from the bootstrap PDFs for each quantity. The two red lines represent fits to the data: $M^*/L_i = (-0.06 \pm 0.48)\log_{10}(M_{500}/10^{14}\,M_\odot) + (1.71 \pm 0.23)$ and $M^*/L_i = -(2.10 \pm 2.01)f_{\rm blue} + (2.17 \pm 0.45)$.

to Zi09 and MAGPHYS being comparable ($M^*/L_i \sim 1.6 \pm 0.2$), to Ip13 yielding the highest stellar mass-to-light ratios ($M^*/L_i \sim 2.4 \pm 0.3$). The sample variance of cluster M^*/L_i is also widest for Zi09 and Ip13, but the differences are small. The cause for these zero-point shifts is a complex combination of underlying IMF choice, SPS modeling, SFH assumption, dust attenuation, etc. Behroozi et al. (2010) as well as Section 4.3 of Leauthaud et al. (2012) address some of these effects. Of these, the choice of IMF generally preserves the power-law slope, but is otherwise a dominant source of systematic bias in $M_\star/L$. For instance, a Salpeter IMF typically gives stellar masses that are 0.25 dex above a Chabrier IMF, the Chabrier being, in turn, also 0.05 dex below a Kroupa IMF (Leauthaud et al. 2012).

The IMF itself may also depend on environment. The Chabrier IMF was originally drawn from field (typically star-forming) galaxies, while the Salpeter IMF is thought to be a better representation of elliptical (more quiescent) systems. Hence, the most appropriate IMF choice might use a combination of a Chabrier IMF for blue systems and a Salpeter IMF for redder systems. For reference, under our analytical framework, the Bell et al. (2003) CMLR with a diet-Salpeter IMF (Table 5) yields $M^*/L_i \sim 2.7 \pm 0.2$ for our sample of clusters, which is in fact comparable to Gonzalez et al.'s (2013) $M^*/L_I = 2.65$ (recall that our Chabrier-MAGPHYS result is $M^*/L_i \sim 1.6 \pm 0.1$).

The detailed physics of stellar evolution is also relevant as the SPS outcomes are especially sensitive to the treatment of bright thermally pulsating asymptotic giant branch (TB-AGB) stars (e.g., Behroozi et al. 2010). Note that Ta11 is based on the dated BC03 SPS package, which does not take TP-AGB into account. Zi09 and MAGPHYS use the CB07 SPS package, which does incorporate TP-AGB evolutionary tracks (Bruzual 2007). Ip13 uses a more recent treatment of the TB-AGB phase, while also considering the effects of circumstellar dust.

Part of the motivation for investigating an assortment of methods for computing total cluster stellar mass is to assess the absolute uncertainty, both statistical and systematic, in such an analysis. To understand these complex systematics, a heuristic approach is to examine the variance in the predictions from a representative set of galaxy SED models varying in their underlying principles/assumptions. We take a first, by no

means definitive, step toward realizing and characterizing the model-dependence of M^*/L_i and M^*/M_{500} (see Section 5.3 and Table 5). We demonstrate that, while absolute scalings and scatters are affected, overall trends exhibited by these stellar-mass quantities do not change appreciably. Thus, we can conclude that, without prior information about the stellar populations (IMF, SFH, etc.), a calculation of the total stellar mass from the mass-to-light conversion ($M^*/L_i = 1.3$–2.7) carries a ∼50% uncertainty. If a specific IMF is well-motivated, Table 6 demonstrates that this systematic uncertainty can be reduced to the ∼10% level.

5.3. Comparison with Previous Studies

As reviewed in Section 1, baryon estimates in clusters often rely on heterogeneous light-to-mass transformations, such as applying a constant dynamical M^*/L (e.g., Gonzalez et al. 2007, 2013; Andreon 2010) to the total cluster luminosities, or galaxy type- or luminosity-dependent M^*/L scaling (e.g., Lin et al. 2003, 2012; Giodini et al. 2009; Dai et al. 2010; Zhang et al. 2011b; Laganá et al. 2011) in summing up the contribution of each galaxy to the cluster stellar mass despite observations that the fraction of blue to red galaxies in clusters can vary significantly (George et al. 2011; Leauthaud et al. 2012).

Following Leauthaud et al. (2012), we make no simplifying assumptions about cluster-wide mass-to-light ratios. Rather, each cluster galaxy and its five-band photometric information is modeled individually, applying either color-dependent luminosity-mass conversion factors or directly deriving stellar masses from SED-fits. By testing a variety of light-to-mass conversion schemes, we can also quantify systematic effects on stellar mass derivations given different stellar population models, stellar formation/evolution scenarios, and galactic environments. We also maximize photo-z information by constructing clusters with a probabilistic membership approach as described in Section 3. Error margins on all measured parameters, conversion schemes, and membership uncertainties have been accounted in the overall error distribution of the final cluster stellar mass quotes.

The first-order relation between cluster-wide M^*/L_i and M_{500}, as captured in Equation (8) for the MAGPHYS results, indicates that the approximation of a constant mass-to-light ratio does *not* introduce systematic errors with respect to cluster size/mass. Furthermore, while one may expect a correlation between M^*/L_i and the blue fraction, we find that the cluster-to-cluster scatter dwarfs this effect (see Equation (8)). The intrinsic spread of M^*/L from the inhomogeneous nature of galaxy population cautions that cluster stellar mass estimates derived from constant light-to-mass factors should use appropriate error margins to account for this population variance.

The present work, Leauthaud et al. (2012), and Kravtsov et al. (2014) are among the few studies using a comparable methodology.[7] Leauthaud et al. (2012) discern the stellar mass fraction of halos based on the COSMOS data using two methods: (1) a cosmological simulation constrained by observations such as the stellar mass function, i.e., halo occupation distribution (HOD)/abundance matching models, and direct X-ray group measurements, akin to this work. Both methods yield comparable results. Leauthaud et al. (2012) infer galaxy stellar masses

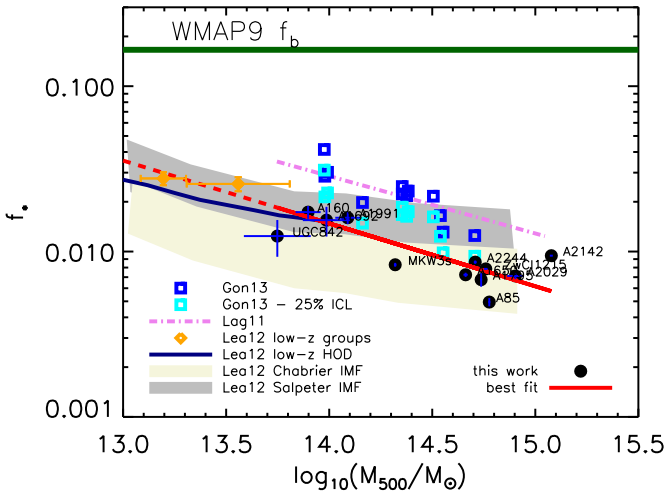

Figure 7. Comparison of $f_\star \equiv M^*/M_{500}$ vs. halo M_{500} from previous studies with our data (MAGPHYS) shown in black. The reference abbreviations are: Gon13 = Gonzalez et al. 2013, Lag11 = Laganá et al. 2011, Lea12 = Leauthaud et al. 2012. For clarity, some error bars, such as those on the Gon13 points, have been omitted. Due to limitation in SDSS photometry, our results likely underestimate the absolute stellar fraction. The cyan squares of Gon13 have a 25% ICL contribution reduction but remain more star-rich than our stellar fractions based on the Chabrier IMF. Lag11's displacement above our work is partly due to systematic offsets in stellar mass (IMF) and total mass between the two works (see discussion in Section 5.3). Orange diamonds are the binned results from Lea12's low-z ($z = [0.22, 0.48]$) groups, which are deemed most comparable to our own study. The HOD fit to the same redshift range is plotted in navy blue. Abundance matching techniques assuming Chabrier and Salpeter IMFs are extensible over a large dynamic range of halo masses, and yield the respective error margins in beige and gray (see Figure 5 in Leauthaud et al. 2012). The best-fit line to our data (in red) has equation $f_{\rm star} = 10^{3.49\pm1.05}(M/M_{500})^{-0.38\pm0.08}$ which, when extrapolated to low halo masses (dotted red), is entirely consistent with Leauthaud et al.'s (2012) observations for groups (orange points). Also note the consistency between our high-mass cluster results and those predicted from fitting cosmological simulations, corroborating the hypothesis that $f_\star$ declines as a single power law from low to high-mass halos. See text for further interpretation.

via individual SED-fits to multi-band COSMOS photometry assuming a Chabrier IMF, as we do with MAGPHYS; and (2) George et al.'s (2011) reliable photo-z based group membership catalog to achieve high completeness above a stellar mass threshold. Two contrasting aspects of our approaches are:

1. Leauthaud et al. (2012) probe more distant systems (i.e., lowest redshift bin is $z \sim 0.22$–0.48, compared to ours $0.04 < z < 0.1$);
2. Leauthaud et al.'s (2012) sample of interest spans $M_{500} \sim 10^{13}$ to 10^{14} $M_\odot$ in the lowest redshift bin, though the theoretical HOD models extend the predicted $f_\star = M^*/M_{\rm tot}$ to $M_{500} \sim 10^{11}$–10^{15} $M_\odot$. Our sample spans the range $M_{500} \sim 10^{14}$–10^{15} $M_\odot$.

The stellar mass buildup between $z \sim 0.3$ and $z \sim 0.1$ is probably not substantial and thus our samples live in comparable regimes. The second point highlights the complementarity of these two studies, which span two orders of magnitude in mass when combined. Our study could also allow a direct comparison for the predicted $f_\star$ versus M_{500} trends of HOD and abundance matching in high-mass regimes that we further address below. In practice, however, relatively shallow SDSS photometry may limit the accuracy of our $f_\star$ measurements (see below).

Figure 7 compares the measured $f_\star$ versus M_{500} relation from several recent studies with the results presented here, focusing exclusively on the MAGPHYS analysis. While varying

[7] Kravtsov et al.'s (2014) sample overlaps with several of our clusters, for which they compute comparable total stellar content within R_{500} when scaled to our mass-to-light ratios, as discussed in this section. Notably, Kravtsov et al. (2014) use a more careful treatment of the BCG surface brightness profiles and caution that cModelMags underestimate total luminosity. See their Table 1.

the assumed IMF (i.e., use of various CMLRs) introduces systematic vertical offsets, it preserves the shape of the trend.

The MAGPHYS M^*/M_{500} ratio exhibits a clear inverse correlation with halo mass M_{500}, corroborating numerous previous reports (e.g., Giodini et al. 2009; Andreon 2010; Zhang et al. 2011b; Lin et al. 2012; Leauthaud et al. 2012; Gonzalez et al. 2013). The best-fit power law is shown in red, with equation:

$$M^*/M_{500} = 10^{3.49\pm1.05}(M_{500}/M_\odot)^{-0.38\pm0.08}. \quad (9)$$

We emphasize that our study cannot account for the entire stellar content of the cluster due to an important limiting factor arising from the photometric data themselves—the SDSS cmodel_mag luminosities are systematically underestimated, especially for bright galaxies with extended profiles (see Hall et al. 2012; Bernardi et al. 2013; Kravtsov et al. 2014), translating into underestimated stellar masses. This factor would also affect the slope of Equation (9) for smaller versus larger clusters; if the luminosities for brighter galaxies are more severely underestimated, and assuming their greater fractional influence in less massive clusters, then the true slope is likely steeper than that observed here. Nevertheless, the apparent consistency with literature (e.g., Figure 7) for our crude $f_\star$ provides additional validation for our methods.

We note that the dark blue points from Gonzalez et al. (2013) include contributions from the "ICL" as defined in their particular study. The ICL-free data, which in the estimation of Gonzalez et al. (2013) are ∼25% below the total cluster stellar mass, are plotted in cyan, constituting a more directly comparable measure to the rest of the works displayed. Gonzalez et al. (2013) is an extension of Gonzalez et al. (2007), with various improvements including a reduction of the (still constant) mass-to-light to $M^*/L_I = 2.65$. Laganá et al. (2011) lies nearly parallel to, but systematically above, our best-fit line, a discrepancy that can be partially ascribed to IMF-induced variations. The study by Laganá et al. uses the luminosity-determined mass-to-light ratio from Kauffmann et al. (2003), which is based on a Kroupa IMF (Kroupa 2001). However, Kroupa IMFs are known to yield only mildly larger stellar masses than Chabrier (0.05 dex), and much less than the Salpeter, whose expected coverage is also overplotted. The remaining discrepancy between our results and those of Gonzalez et al. (2013) and Laganá et al. (2011) may be due to incorrect subtraction of the background and improper modeling of the outer light profile, which is a known issue in SDSS "cmodel" magnitudes (Bernardi et al. 2013; Kravtsov et al. 2014)—we will return to this point in Section 5.4. An additional source of the tension between our results and those of Laganá et al. (2011) is our different estimates of the total halo mass. For clusters that overlap between our samples, we find factors of 10–30% difference between our measurements of M_{500}, with measurements from Laganá et al. (2011) being systematically lower (resulting in higher $f_\star$ estimates). Recent work has demonstrated that cluster masses based on *XMM-Newton*-derived scaling relations may be biased low by a factor of ∼30% (see, e.g., von der Linden et al. 2014b), which would explain most of the offset between our $f_\star$–M_{500} relations. Other factors, such as cluster sample variance and the use of oversimplified mass-to-light ratios and cluster member accounting, may also contribute to these systematic offsets.

Figure 7 shows that our results naturally extend the power-law of Leauthaud et al.'s lower-mass galaxy groups over the range $M_{500} \sim 10^{13}$–10^{15} $M_\odot$, essentially consistent with the Charbrier extrapolation of models from abundance matching in Leauthaud et al. This suggests that (1) the relevant physics of galaxy groups transitions smoothly to massive clusters, hence both may be studied under the same framework; (2) if universal baryon fractions, $f_b = f_{\rm gas} + f_\star$, are constant with cluster scale to first order, then the trend of declining stellar mass fraction in increasingly more massive halos implies that $M^*/M_{\rm gas}$ is lower for higher-mass cluster systems. In turn, this suggests that baryon cooling would be less efficient in deeper potential wells; and (3) the lower absolute scaling of total stellar fractions than previous expectations (due primarily to different choices of IMF) makes explaining the baryon fraction deficiency with respect to *WMAP*'s cosmic measurements increasingly challenging. These interpretations should be read with the caveat that our absolute stellar masses likely represent underestimates of their true values.

5.4. Methodological Uncertainties and Incompleteness

Stellar mass estimates for individual galaxies remain poorly constrained (Courteau et al. 2014). For galaxy clusters, systematic and statistical pitfalls due to stellar evolution modeling (Behroozi et al. 2010) combined with membership uncertainty make the assessment of the total stellar mass even less certain. Still, once it is recognized that systematics dominate over statistical uncertainties in stellar mass measurements (see Section 4.3 in Leauthaud et al. 2012), the latter can be assessed given the former as background and the error margins can be separately decoupled. For instance, errors attributable to stellar population modeling systematics can be probed by repeating our methodology for a number of different stellar light-to-mass conversion techniques, bootstrapping over all statistical errors associated with the particular technique. The range of results for a representative pool of such techniques indicates the nature of the systematic variation due to the assumptions of the conversion scheme. In this work, we have mostly explored these systematic effects by supplementing MAGPHYS calculations with several popular CMLRs.

The uncertainty due to the cluster member accounting (see Section 3) is now examined. Deprojection effects amount to less than a 15% downward adjustment from selecting galaxies in a cylinder to a sphere in redshift space (Leauthaud et al. 2012). In Section 3 we further quantify this bias as a function of spectroscopic completeness, showing that our cluster membership algorithm is likely biased by <20% for systems with spectroscopic completeness >10%. The photometric redshift probability distribution has an uncertainty that can also be characterized by applying different prob(z) catalogs (if available to the same field) and inspecting the resulting variance. This error source is limited by the reliability of the externally supplied form of prob(z) for a cluster field. A first-order estimate of the error associated with using photometric redshifts can be made by isolating the spectroscopic subset of cluster candidates and performing the entire analysis on these galaxies alone. These galaxies have unambiguous true redshifts and membership designations, making their aggregation a benchmark for comparing the accuracy of calculations based on photometric redshifts. We then re-compute the parameters using our statistical treatment of $z_{\rm phot}$ estimates (Section 3) and compare the two outcomes. Figure 8 shows the differences between the photometric and spectroscopic redshift-based calculations of median M^*/L_i as function of halo mass, M_{500}. The mass-to-light ratios inferred using only photometric redshifts tend to be underestimated with respect to those computed using spectroscopic redshifts. The median bias of ∼0.15 $M_\odot/L_{i,\odot}$ is similar in magnitude to the typical uncertainty for a given cluster M^*/L_i.

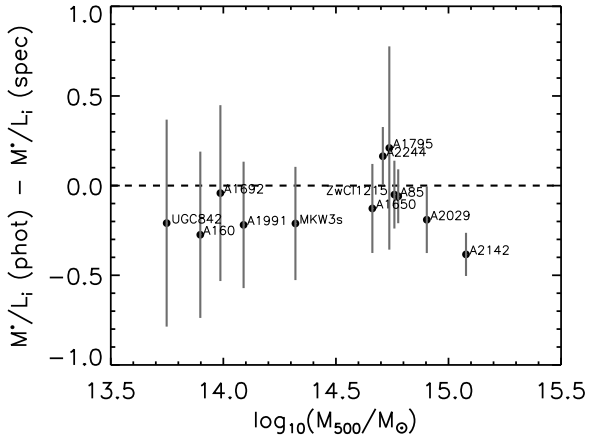

Figure 8. Expected stellar mass-to-light ratio bias if the $z_{\rm phot}$ probability distributions used in this work were not supplemented by $z_{\rm spec}$ measurements. For this exercise, we re-construct each cluster using only the subset of candidate galaxies with both spectroscopic and photometric redshifts. We sum MAGPHYS-derived stellar masses via the probabilistic methodology described in Section 3, once using exclusively spectroscopic redshifts, and once using photometric. For the subsample with definitive membership assignment using spectroscopic redshift measurements, photometric redshift alone appears to yield systematically lower mass-to-light ratios, by $\sim$0.15 $M_{\odot}/L_{\odot}$, which is similar to the uncertainty in the calculated M^*/L_i.

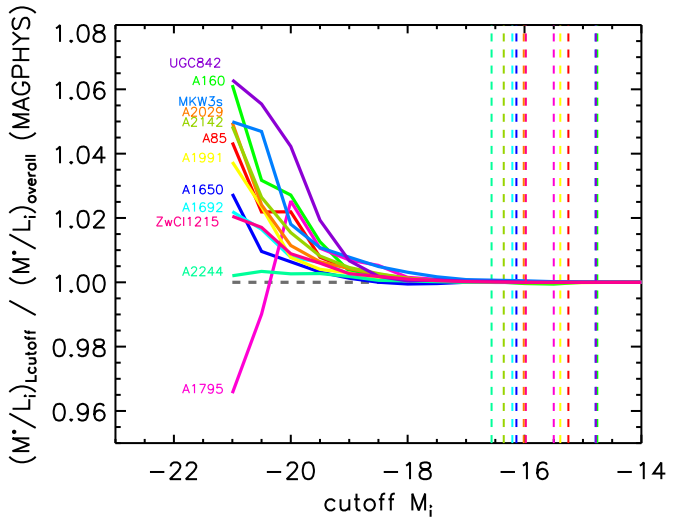

Figure 9. Convergence of mass-to-light ratios to their final values as a function of absolute magnitude limit of cluster galaxy detection. Having all cluster galaxies brighter than $M_i = -19$ already anchors the overall M^*/L_i to within 1%. The convergence is settled by $M_i = -17$, which is not a stringent requirement for nearby systems (see text). Vertical dashed lines mark the approximate positions of limiting absolute i-magnitudes corresponding $r < 22$ for each cluster redshift, assuming $r - i \approx 0.3$.

Another possible source of bias, as we have alluded to in previous sections, is the use of "cmodel" magnitudes from the SDSS pipeline. Bernardi et al. (2013) showed that roughly 20% of the total stellar mass density at $z \sim 0.1$ is missing in SDSS cmodel magnitudes, with the differences being largest at the high mass end. Since galaxy clusters tend to have a higher fraction of massive galaxies, this bias could be even higher for our sample. In the most extreme case—that of a galaxy cluster with $M_{500} \sim 10^{14}\ M_{\odot}$, where the BCG contributes a substantial fraction of the total mass—this could bias our estimate of M_* low by 35%–40%. In an attempt to determine the maximal effect of this bias on the measured M_*/L_i, we can assume that the stellar populations in the outer halo of galaxies (where "cmodel" magnitudes underestimate the flux) are exceptionally young ($M_*/L_i = 1.0$). This extreme scenario, combined with the maximal bias of 35%–40% mentioned above, would lead to a bias in M_*/L_i of 15%. Of course, this scenario is also unrealistic, as Roediger et al. (2011) has shown that Virgo cluster galaxies have relatively flat age and metallicity gradients in their outskirts. However, this calculation shows that any bias due to the use of "cmodel" magnitudes rather than those, for example, presented in Bernardi et al. (2013), is likely <15%.

Mass incompleteness, due to the magnitude-limited nature of surveys, is also a source of concern. Luminosity function fits (e.g., Schechter 1976) have often been invoked to estimate the contribution of undetected galaxy members below a luminosity threshold. We choose not to extrapolate our LFs because (1) faint-end slopes are poorly constrained, and (2) the gain in accuracy for our present purpose is minimal. To substantiate the latter claim, note that, being nearby ($z < 0.1$), our clusters are well sampled by the SDSS: our magnitude limit of $r < 22$ mag corresponds to 0.01 $L_{\star}$.

Recall that our primary goal is to characterize cluster-wide stellar mass-to-light ratios which, being a weighted average, does not require a complete accounting of all galaxies present (as long as the missing galaxies do not deviate significantly from the mean). In order to determine how deep a given survey must be for the uniform-M^*/L_i approximation to be suitable, we show in Figure 9 the derived M^*/L_i as a function of the survey depth. Firstly, note the range spanned by the ordinate. Detection of all galaxy members brighter than $M_i = -19$ ensures that M^*/L_i falls within 1% of the final value, despite the fact that the vast majority of the galaxies we detect in each cluster are fainter than this limit. For a cluster at $z = 0.1$, this corresponds to a magnitude limit of $m_i = 19.3$ mag, which is certainly attainable by SDSS. The rapid convergence of this plot, which occurs well clear of our survey limits, suggests that faint-end incompleteness does not affect our conclusions regarding cluster M^*/L.

We conclude our discussion on uncertainties by advocating the use of multi-wavelength photometry (such as COSMOS) for stellar mass estimates whenever possible. In the absence of exceptionally well-sampled photometry spanning the optical through IR (e.g., COSMOS, CLASH; Leauthaud et al. 2012; Postman et al. 2012), we recommend at least three photometric bands which span the 4000 Å break, which will allow a coarse modeling of the SED, yielding improved constraints on M^*/L_i over CMLRs.

6. CONCLUSION

We have presented an investigation of the stellar mass budget for galaxy clusters in the total mass range $M_{500} \sim 10^{13}$–$10^{15}\ M_{\odot}$. We specifically addressed the distribution of overall cluster mass-to-light ratio values, and the total stellar mass in galaxies as a fraction of total halo mass for clusters of various sizes. Toward this end, we have developed a bootstrapping algorithm for cluster stellar mass accounting on a galaxy-by-galaxy basis in the absence of complete spectroscopic field coverage as an alternative to statistical, flux-based background subtraction methods. Our method can be applied to any photometric redshift catalog and stellar light-to-mass conversion models, making it valuable in assessing model-dependent systematic uncertainties. We have repeated our tests with several widely cited color–mass-to-light relations (CMLRs) and also using full SED-fitting with the program MAGPHYS utilizing five-band optical photometry from SDSS. Our results are summarized below:

1. We find no strong evidence for first-order dependence of cluster-wide M^*/L_i on halo mass. Cluster mass-to-light ratios span relatively narrow ranges ($\pm 10\%$) with the absolute level and intrinsic variance set by the specifics of the stellar population models (see Figure 6 and Table 6 for these results). Not surprisingly, M^*/L_i is found to weakly correlate (Pearson $R = -0.53$) with cluster blue fraction, though an expanded cluster sample is required for a more precise quantification of this statement.

   We have shown that the acceptable range of M^*/L_i ratios varies as a function of the preferred IMF and SPS packages, but those are essentially independent of the halo mass. For the popular Chabrier IMF coupled with the CB07 SPS prescription, we advocate a MAGPHYS value of $M^*/L_i \approx 1.7 \pm 0.2$ for galaxy clusters. For a (diet) Salpeter IMF, a higher M^*/L_i value of $\sim$2.7 may be more appropriate for the same clusters. The truth likely lies in between.
2. Despite limitations of our present total stellar mass estimates, which make them imperfect for accurate cluster stellar content accounting, we measure a strong correlation between the cluster stellar-halo mass fraction ($f_\star$) and halo mass. Such a trend supports the emerging consensus that star formation is less efficient in deeper potential wells (e.g., Lin et al. 2003; Gonzalez et al. 2013). Our SED-fitting analysis based on MAGPHYS also yields $f_\star = 10^{3.49\pm1.05}(M/M_{500})^{-0.38\pm0.08}$ in agreement with previous studies. The zero-point of this relation depends on the adopted CMLR or SED-fit for the stellar mass determinations, but the slope is preserved. A declining stellar mass fraction with increasing halo mass has yet to be reconciled with theoretical predictions. See Gonzalez et al. (2013) and discussion therein.

Our study is similar in spirit to that of Leauthaud et al. (2012), who compute stellar masses and mass-to-light ratios for galaxy groups in the COSMOS survey. As illustrated in Figure 7, our results form a smooth extension (to higher mass) of their work, corroborating the notion that stars may contribute even less to the cluster baryon budgets than previously expected, especially in massive halos.

We have restricted our study to nearby galaxy clusters, but the methodology described here can be easily extended to a wide range of redshifts and data sets, provided that the photometric redshifts are reliable and the photometry is relatively deep ($M_{i,\mathrm{lim}} < -19$ mag).

We are grateful to the anonymous referee for the thoughtful suggestions, which improved the content and clarity of this paper. Y.S. and S.C. are grateful to the Natural Science and Engineering Research Council of Canada for funding via an Undergraduate Summer Research Award and Research Discovery Grant, respectively, which made this study possible. M.M. acknowledges support provided by NASA through a Hubble Fellowship grant from STScI. Comments from Anthony Gonzalez on an earlier draft were most helpful. We also thank Larry Widrow, Joel Roediger, Carlos Cunha, and John Moustakas for constructive suggestions at various stages of this project.

Funding for SDSS-III has been provided by the Alfred P. Sloan Foundation, the Participating Institutions, the National Science Foundation, and the U.S. Department of Energy Office of Science. The SDSS-III Web site is http://www.sdss3.org/.

SDSS-III is managed by the Astrophysical Research Consortium for the Participating Institutions of the SDSS-III Collaboration including the University of Arizona, the Brazilian Participation Group, Brookhaven National Laboratory, Carnegie Mellon University, University of Florida, the French Participation Group, the German Participation Group, Harvard University, the Instituto de Astrofisica de Canarias, the Michigan State/Notre Dame/JINA Participation Group, Johns Hopkins University, Lawrence Berkeley National Laboratory, Max Planck Institute for Astrophysics, Max Planck Institute for Extraterrestrial Physics, New Mexico State University, New York University, Ohio State University, Pennsylvania State University, University of Portsmouth, Princeton University, the Spanish Participation Group, University of Tokyo, University of Utah, Vanderbilt University, University of Virginia, University of Washington, and Yale University.

REFERENCES

Ahn, C. P., Alexandroff, R., Allende Prieto, C., et al. 2014, APJS, 211, 17
Akritas, M. G., & Bershady, M. A. 1996, ApJ, 470, 706
Allen, S. W. 1998, MNRAS, 296, 392
Allen, S. W., Schmidt, R. W., Ebeling, H., Fabian, A. C., & van Speybroeck, L. 2004, MNRAS, 353, 457
Allen, S. W., Schmidt, R. W., & Fabian, A. C. 2002, MNRAS, 334, L11
Andreon, S. 2010, MNRAS, 407, 263
Andreon, S., & Hurn, M. 2010, MNRAS, 404, 1922
Arnouts, S., Walcher, C. J., Le Fvre, O., et al. 2007, A&A, 476, 137
Bartelmann, M., & Schneider, P. 2001, PhR, 340, 291
Behroozi, P. S., Conroy, C., & Wechsler, R. H. 2011, ApJ, 717, 379
Bell, E., & de Jong, R. 2001, ApJ, 550, 212
Bell, E., Mcintosh, D. H., Katz, N., & Weinberg, M. D. 2003, ApJS, 149, 289
Bernardi, M., Meert, A., Sheth, R., et al. 2013, MNRAS, 436, 697
Bolzonella, M., Miralles, J.-M., & Pelló, R. 2000, A&A, 363, 476
Bruzual, A., & Charlot, S. 2003, MNRAS, 344, 1000
Bruzual, A. G. 1983, ApJ, 273, 105
Bruzual, A. G. 2007, in ASP Conf. Ser. 374, From Stars to Galaxies: Building the Pieces to Build up the Universe, ed. A. Vallenari et al. (San Francisco, CA: Asp), 303
Bruzual, A. G., & Charlot, S. 1993, ApJ, 405, 538
Calzetti, D., Armus, L., Bohlin, R. C., et al. 2000, ApJ, 533, 682
Cappellari, M., Bacon, R., Bureau, M., et al. 2006, MNRAS, 366, 1126
Carliles, S., Budavri, T., Heinis, S., et al. 2010, ApJ, 712, 511
Chabrier, G. 2003, PASP, 115, 763
Charlot, S., & Fall, S. M. 2000, ApJ, 539, 718
Conroy, C. 2013, ARA&A, 51, 393
Conroy, C., & Gunn, J. 2010, ApJ, 712, 833
Conroy, C., Gunn, J., & White, M. 2009, ApJ, 699, 486
Courteau, S., Cappellari, M., de Jong, R. S., et al. 2014, RvMP, 86, 47
Csabai, I., Dobos, L., Trencséni, M., et al. 2007, AN, 328, 852
da Cunha, E., Charlot, S., & Elbaz, D. 2008, MNRAS, 388, 1595
Dai, X., Bregman, J. N., Kochanek, C. S., & Rasia, E. 2010, ApJ, 719, 119
De Lucia, G., Springel, V., White, S. D. M., Croton, D., & Kauffmann, G. 2006, MNRAS, 366, 499
de Vaucouleurs, G. 1948, AnAp, 11, 247
Driver, S. P., Norberg, P., Baldry, I. K., et al. 2009, A&G, 50, 5.12
Duffy, A., Shaye, J., Kay, S., et al. 2008, MNRAS, 390, L64
Dunkley, J. 2009, ApJS, 180, 306
Fioc, M., & Rocca-Volmerange, B. 1997, A&A, 326, 950
Gallazzi, A., & Bell, E. 2009, ApJS, 185, 253
George, M., Leauthaud, A., Bundy, K., et al. 2011, ApJ, 742, 125
Giodini, S., Pierini, D., Finoguenov, A., et al. 2009, ApJ, 703, 982
Gonzalez, A. H., Zabludoff, A. I., & Zaritsky, D. 2005, ApJ, 618, 195
Gonzalez, A. H., Zaritsky, D., & Zabludoff, A. I. 2007, ApJ, 666, 147
Gonzalez, A. H., Sivanandam, S., Zabludoff, A. I., & Zaritsky, A. H. 2013, ApJ, 778, 14
Hall, M., Courteau, S., Dutton, A. A., McDonald, M., & Zhu, Y. 2012, MNRAS, 425, 2741
High, F. W., Hoekstra, H., Leethochawalit, N., et al. 2012, ApJ, 758, 68
High, F. W., Stalder, B., Song, J., et al. 2010, ApJ, 723, 1736
Hoyle, B., Masters, K. L., Nichol, R. C., Jimenez, R., & Bamford, S. 2012, MNRAS, 423, 3478
Into, T., & Portinari, L. 2013, MNRAS, 430, 2715

Jones, C., & Forman, W. 1999, ApJ, 511, 65
Kaiser, N., Squires, G., & Broadhurst, T. 1995, ApJ, 449, 460
Kauffmann, G., Heckman, T. M., White, S. D. M., et al. 2003, MNRAS, 341, 33
Kennicutt, R. 1983, ApJ, 272, 54
Komatsu, E., Smith, K. M., Dunkley, J., et al. 2011, ApJS, 192, 18
Kravtsov, A. V., Nagai, D., & Vikhlinin, A. A. 2005, ApJ, 625, 588
Kravtsov, A., Vikhlinin, A., & Meshscheryakov, A. 2014, arXiv:1401.7329v1
Kroupa, P. 2001, MNRAS, 322, 231
Laganá, T. F., Zhang, Y.-Y., Reiprich, T. H., & Schneider, P. 2011, ApJ, 743, 13
Leauthaud, A., George, M. R., Behroozi, P. S., et al. 2012, ApJ, 746, 95
Lin, Y., Mohr, J. J., & Stanford, S. A. 2003, ApJ, 591, 749
Lin, Y., Stanford, S. A., Eisenhardt, P., et al. 2012, ApJ, 745, L3
Lupton, R. H. 2005, Sloan Technical Papers
Maraston, C. 2005, MNRAS, 362, 799
Mariago, P., & Girardi, L. 2007, A&A, 370, 194
Miller, C. J., Nichol, R. C., Reichart, D., et al. 2005, AJ, 130, 968
Mohr, J. J., Mathiesen, B., & Evrard, A. E. 1999, ApJ, 517, 627
Planck Collaboration, Ade, P. A. R., et al. 2014, A&A, 571, A16
Postman, M., Coe, D., Benítez, N., et al. 2012, ApJS, 199, 25
Roediger, J. C., Courteau, S., MacArthur, L. A., & McDonald, M. 2011, MNRAS, 416, 1996
Salpeter, E. E. 1955, ApJ, 121, 161
Schechter, P. 1976, ApJ, 203, 297
Schneider, P. 2006, Extragalactic Astronomy and Cosmology (New York: Springer)
Springel, V., White, S. D. M., Jenkins, A., et al. 2005, Natur, 435, 629
Stoughton, C., Lupton, R. H., Bernardi, M., et al. 2002, AJ, 123, 485
Sun, M., Voit, G.M., Donahue, M., et al. 2009, ApJ, 693, 1142
Szabo, T., Pierpaoli, E., Dong, F., Pipino, A., & Gunn, J. 2011, ApJ, 736, 21
Taylor, E. N., Hopkins, A. M., Baldry, I. K., et al. 2011, MNRAS, 418, 1587
Tinsley, B., & Gunn, J. 1976, ApJ, 203, 52
Tinsley, B. M. 1978, ApJ, 222, 14
van der Marel, R. P. 1991, MNRAS, 253, 710
Vikhlinin, A., Burenin, R. A., Ebeling, H., et al. 2009, ApJ, 692, 1033
Vikhlinin, A., Kravtsov, A., Forman, W., et al. 2006, ApJ, 640, 691
Voit, G. M. 2005, RvMP, 77, 207
von der Linden, A., Allen, M. T., Applegate, D. E., et al. 2014a, MNRAS, 439, 2
von der Linden, A., Mantz, A., Allen, S. W., et al. 2014b, MNRAS, 443, 1973
Walcher, C. J., Groves, B., Budavri, T., & Dale, D. 2011, Ap&SS, 331, 1
White, D. A., Jones, C., & Forman, W. 1997, MNRAS, 292, 419
White, S. D. M., Navarro, J. F., Evrard, A. E., & Frenk, C. S. 1993, Natur, 366, 429
Zhang, Y.-Y., Andernach, H., Caretta, C., et al. 2011a, A&A, 526, A105
Zhang, Y.-Y., Lagan, T. F., Pierini, D., et al. 2011b, A&A, 535, A78
Zibetti, S., Charlot, S., & Rix, H.-W. 2009, MNRAS, 400, 1181